Supplementary Information

Spectroscopic Investigations of [FeFe] Hydrogenase Maturated with $[^{57}Fe_2(adt)(CN)_2(CO)_4]^{2-}$

Ryan Gilbert-Wilson[#†], Judith F. Siebel[#‡], Agnieszka Adamska-Venkatesh[‡], Cindy C. Pham[¶], Edward Reijerse[‡], Hongxin Wang[¶∞], Stephen P. Cramer[¶∞]*, Wolfgang Lubitz[‡]*, Thomas B. Rauchfuss[†]*

[†]School of Chemical Sciences, University of Illinois at Urbana-Champaign, Urbana, Illinois 61801, United States

[‡]Max-Planck-Institut für Chemische Energiekonversion, Stiftstrasse 34-36,

45470 Mülheim an der Ruhr, Germany

[¶] Department of Chemistry, University of California, Davis, California 95616, United States

[∞]Physical Biosciences Division, Lawrence Berkeley National Laboratory, Berkeley, California 94720, United States

Table of Contents

Experimental Details

General Considerations. Unless otherwise indicated, reactions were conducted using standard Schlenk techniques or in a glove box under an N_2 atmosphere at room temperature with stirring. Elemental sulfur, 37% solution of formaldehyde, potassium metal, anthracene, tetraethyl ammonium cyanide and ammonium chloride were obtained from Aldrich and used as received. Cylinders of carbon monoxide were obtained from SJ Smith and used as received. ^{57}Fe metal powder was purchased from Isoflex and used as received. ^{13}C (150.6 MHz) spectra were acquired in a Varian UNITY Inova 600. ESI-MS data for compounds were acquired using a Waters Micromass Quattro II spectrometer.

Synthesis of $^{57}FeBr_2$: $^{57}FeBr_2$ was synthesized by modification of a literature procedure for $FeBr_2$ synthesis.[1] ^{57}Fe metal (501 mg, 8.80 mmol) and a small stirrer bar were transferred to a Schlenk flask under an argon atmosphere. A septa and a needle with attached bubbler were attached to the flask. Fresh concentrated hydrobromic acid (48%, 2.5 mL) was then transferred to the flask by syringe resulting in hydrogen evolution. Once hydrogen evolution had slowed the septa was replaced with a glass stopper and the flask was heated to 80 °C with stirring for 2 hours. The solution was then allowed to cool to room temperature and methanol (5 mL) was added. The solvents were then removed under vacuum. The remaining white/yellow solid was heated at 100 °C under a vacuum of 10 torr for 4 hours, with the end point identified as the point when a piece of dry ice applied to the side of the flask did not condense any methanol. Note: Previous tests with $FeBr_2$ indicated increased temperatures or stronger vacuum led to sublimation of $FeBr_2$ out of the flask into the attached trap. The flask was allowed to cool to room temperature under vacuum and then moved to the glovebox where the pale yellow solid was collected to yield $^{57}FeBr_2$ (1.82 g, 8.40 mmol, 95% yield).

Synthesis of $^{57}Fe_2S_2(CO)_6$: Description in the main text.

Synthesis of $^{57}Fe_2(adt)(CO)_6$: $^{57}Fe_2(adt)(CO)_6$ was synthesized by modification of a literature procedure for $Fe_2(adt)(CO)_6$ synthesis.[2]

(a) Aminomethylation reagent. Aminomethylation reagent was prepared fresh before use. Ammonium carbonate (450 mg, 4.68 mmol) was placed under an argon atmosphere, followed by the addition of THF (6 mL). The resulting suspension was stirred and heated to 60 °C, at which point a septa and needle with bubbler were attached to the flask and a 37% solution of formaldehyde was added (5.0 mL, 67 mmol) resulting in significant gas evolution. The resulting clear solution was stirred at 60 °C and then allowed to cool to room temperature.

(b) $^{57}Fe_2(adt)(CO)_6$. $^{57}Fe_2S_2(CO)_6$ (180 mg, 0.524 mmol) in THF (10 mL) was cooled to -77 °C. 1.07 mL of a 1 M solution of $LiBEt_3H$ (1.07 mmol) was then added dropwise, inducing a color change to brown and eventually green. The solution was then allowed to warm to -40 °C and stirred at -40 °C causing a color change to brown/red. The solution was then cooled back to -77 °C and CF_3COOH (85 µL, 1.14 mmol) was added dropwise over a period of 10 minutes resulting in a color change to a lighter red. The solution was then allowed to warm to room temperature and was then cannula transferred into the aminomethylation solution which had been pre-chilled to 0 °C, causing a color change to

darker red. The solution was allowed to slowly warm to room temperature and stirred for 12 hours. The solvent was then removed under vacuum to leave a red and white residue. The flask was refilled with argon and dichloromethane (10 mL) was added. From this point manipulations were performed in air. The mixture was sonicated and the red solution decanted. The residue was extracted again with dichloromethane (2 x 10 mL) and all extracts were combined and filtered through celite. The solution was then evaporated under reduced pressure to leave a bright red residue, which was subsequently extracted with a 4:1 mixture of hexane:dichloromethane (3 x 2 mL) and chromatographed on a 2 x 30 cm silica gel column. Elution with hexanes gave an orange first band which was identified by IR spectroscopy as $^{57}Fe_2S_2(CO)_6$ (5 mg). Increasing the polarity to 4:1 hexane:dichloromethane gave elution of a red second band which remains unidentified. A further slow shift in the polarity to an eventual concentration of 1:1 hexane:dichloromethane led to elution of a bright red third band which consisted of $^{57}Fe_2(adt)(CO)_6$ (58.0 mg, 0.149 mmol, 28% yield). IR (pentane): $\nu_{C\equiv O}$ = 2076 (s), 2036 (s), 2008 (s), 1990 (s), 1980 (m); ^{13}C NMR (600 MHz, d_8-Toluene, 60 $^{\circ}$C): δ 208.03 (d, $J_{C\text{-}Fe}$ = 26.4 Hz, **C**O); 45.25 (s, **C**H_2).

Synthesis of $(Et_4N)_2[^{57}Fe_2(adt)(CN)_2(CO)_4]$: $(Et_4N)_2[^{57}Fe_2(adt)(CN)_2(CO)_4]$ was synthesized by modification of a literature procedure for $(Et_4N)_2[Fe_2(adt)(CN)_2(CO)_4]$.[3] $(Et_4N)CN$ (26.2 mg, 0.168 mmol) was dissolved in acetonitrile (1.5 mL) under a glove box atmosphere. A solution of $^{57}Fe_2(adt)(CO)_6$ (32.6 mg, 0.084 mmol) in acetonitrile (1.5 mL) was then added to the flask with stirring leading to a small amount of CO evolution, once this ceased the flask was sealed and allowed to stir for 10 hours. The solvent was removed under vacuum to give a bright red solid. THF (2 mL) was then added and the mixture thoroughly agitated. The red solid was then collected and washed again with THF (2 mL) and pentane (2 x 3 mL) before drying to yield $(Et_4N)_2[^{57}Fe_2(adt)(CN)_2(CO)_4]$ (50.1 mg, 0.078 mmol, 93% yield). MS ESI-(m/z) 515.6 ($(Et_4N)[^{57}Fe_2(adt)(CN)_2(CO)_4]^-$) IR (acetonitrile): $\nu_{C\equiv N}$ = 2075 (m) $\nu_{C\equiv O}$ = 1968 (s), 1924 (s), 1891 (s), 1873 (sh)

Mass Spectrometry

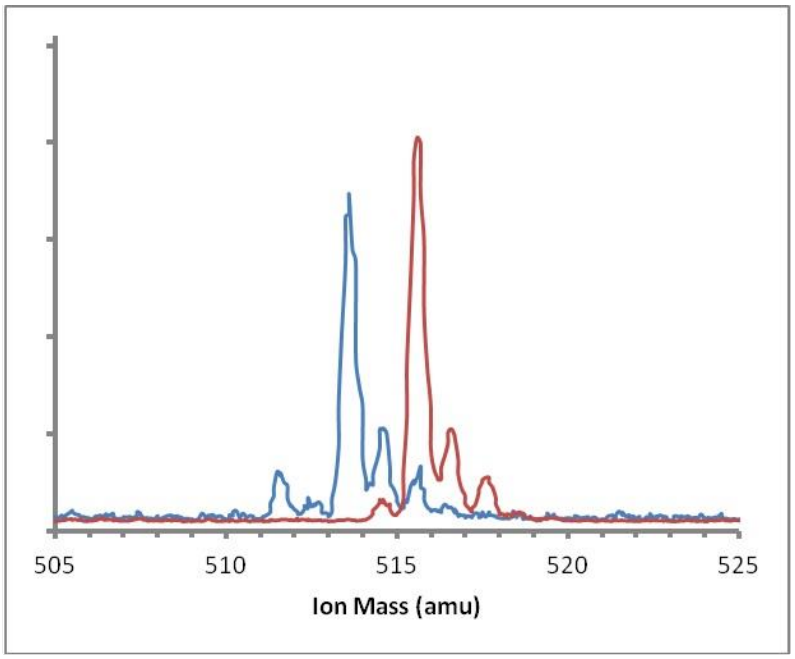

Figure S1. Negative ion mass spectrometry plot of the $(Et_4N)[Fe_2(adt)(CN)_2(CO)_4]^-$ (blue) and $(Et_4N)[^{57}Fe_2(adt)(CN)_2(CO)_4]^-$ (red) ions overlaid.

Negative ion ESI mass spectrometry was used to confirm the successful incorporation of ^{57}Fe into $(Et_4N)_2[^{57}Fe_2(adt)(CN)_2(CO)_4]$. This was achieved through a comparison with the unlabeled cluster $(Et_4N)_2[Fe_2(adt)(CN)_2(CO)_4]$. The major ion detected was the tetraethylamine-cluster ion pair with a single negative charge. As can be observed in Figure S1 there is a clear 2 mass unit shift for the labeled cluster vs. the unlabeled cluster, demonstrating the shift from a sample containing largely ^{56}Fe versus the labeled spectra which contains ^{57}Fe almost exclusively.

^{13}C NMR of ^{57}Fe Clusters

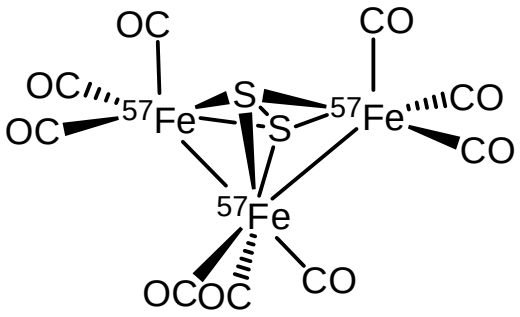

$J_{C\text{-}Fe}$ = 26.3 Hz

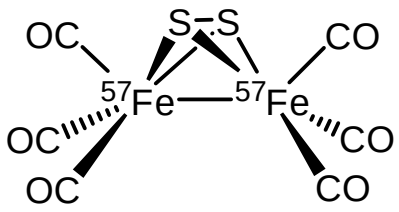

$J_{C\text{-}Fe}$ = 28.3 Hz

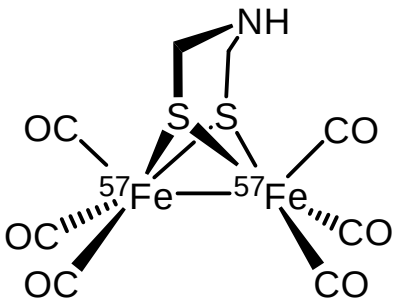

$J_{C\text{-}Fe}$ = 26.4 Hz

Chart S1. Iron sulfur carbonyl clusters synthesized with $J_{C\text{-}Fe}$ coupling constants.

H_{ox}-CO State Preparation

FTIR spectroscopy was used to follow the preparation of the H_{ox}-CO state of HydA1. FTIR measurements were carried out using a Bruker IFS 66v/s FTIR spectrometer equipped with a nitrogen cooled Bruker mercury cadmium telluride (MCT) detector. The spectra were accumulated in the double-sided, forward-backward mode with 1000 scans (14 min) and a resolution of 2 cm^{-1} at 15 °C. Data processing was facilitated by home written routines in the MATLAB™ programming environment.

The FTIR spectrum obtained from freshly maturated HydA1 with $[^{57}Fe_2(adt)(CN)_2(CO)_4]^{2-}$ exhibits a mixture of signals originating from all active and CO inhibited redox states (Figure S2B). Upon oxidation of HydA1 with thionine (ratio 1:1) only a mixture of H_{ox} and H_{ox}-CO states is present (Figure S2C) that allows generating a pure H_{ox}-CO state after flushing the sample for 20 minutes with CO gas (Figure S2D).

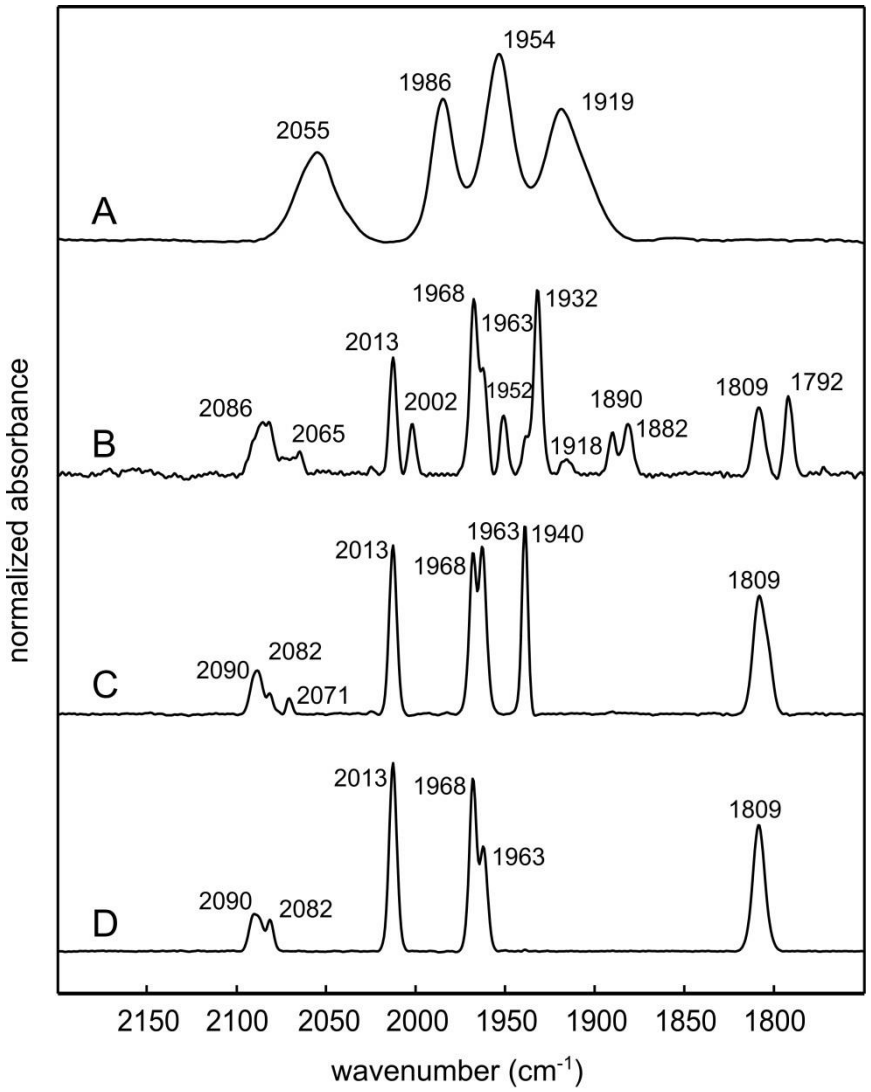

Figure S2. Normalized FTIR spectra recorded for the $(Et_4N)_2[^{57}Fe_2(adt)(CN)_2(CO)_4]$ precursor (A) and HydA1 selectively labeled with ^{57}Fe at the $[2Fe]_H$ subunit of the H-cluster (B-D) recorded at 15 °C. (B) as obtained from maturation, (C) oxidized with thionine, (D) oxidized with thionine and flushed with CO gas.

Selective ^{57}Fe-Labeling of the [4Fe-4S]$_H$ Cluster

For activity measurements, $[Fe_2(adt)(CN)_2(CO)_4]^{2-}$ was added to reconstituted unmaturated HydA1 as described earlier.[4] Reconstituted HydA1 maturated with $[Fe_2(adt)(CN)_2(CO)_4]^{2-}$ showed an H_2 oxidation activity of 136 ± 2 s^{-1} as observed before for as-isolated HydA1 maturated with $[Fe_2(adt)(CN)_2(CO)_4]^{2-}$.[4] Figure S3 shows the UV spectrum of as-isolated unmaturated HydA1 before any treatment (blue) and after unfolding (green). Unfolding leads to absence of the broad absorption shoulder from 300–550 nm, clearly showing the absence of any [4Fe-4S]$_H$ cluster. After reconstitution with $^{57}FeCl_3$ and Na_2S followed by desalting, the absorption of the [4Fe-4S]$_H$ cluster is re-established (red). As shown in the Figure S4 the EPR signal of as-isolated unmaturated HydA1 in the presence of sodium dithionate (blue) is characterized by the same g-values as reconstituted unmaturated HydA1 (red) under the same conditions.

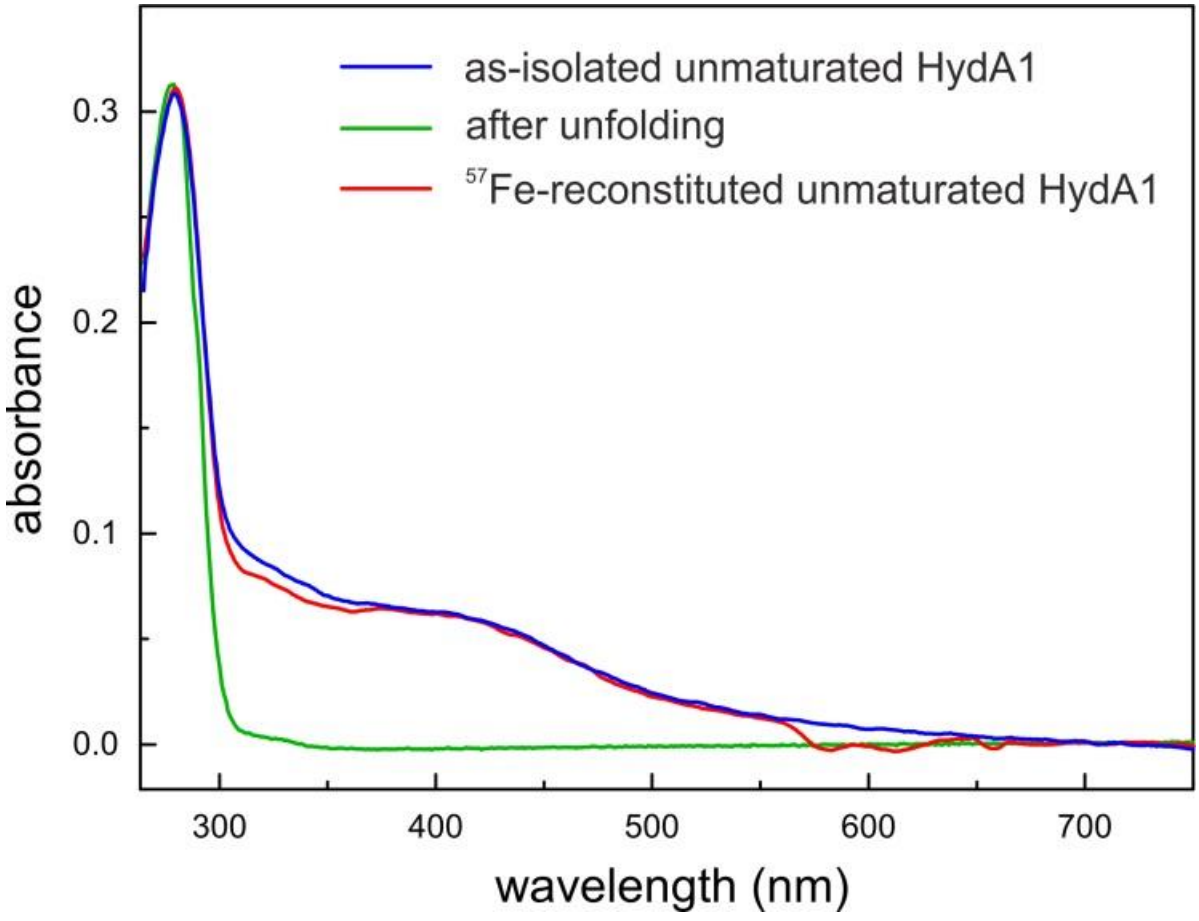

Figure S3. UV spectrum of as-isolated unmaturated HydA1 (blue), after treatment with 6 M guanidium chloride (green) and ^{57}Fe-reconstituted unmaturated HydA1 (red). The spectra were measured in 100 mM Tris/HCl, pH 8.0 and 150 mM NaCl at room temperature using an Ocean Optics USB2000+XR1-ES, equipped with a DH-MINI Deuterium Tungsten Halogen Source.

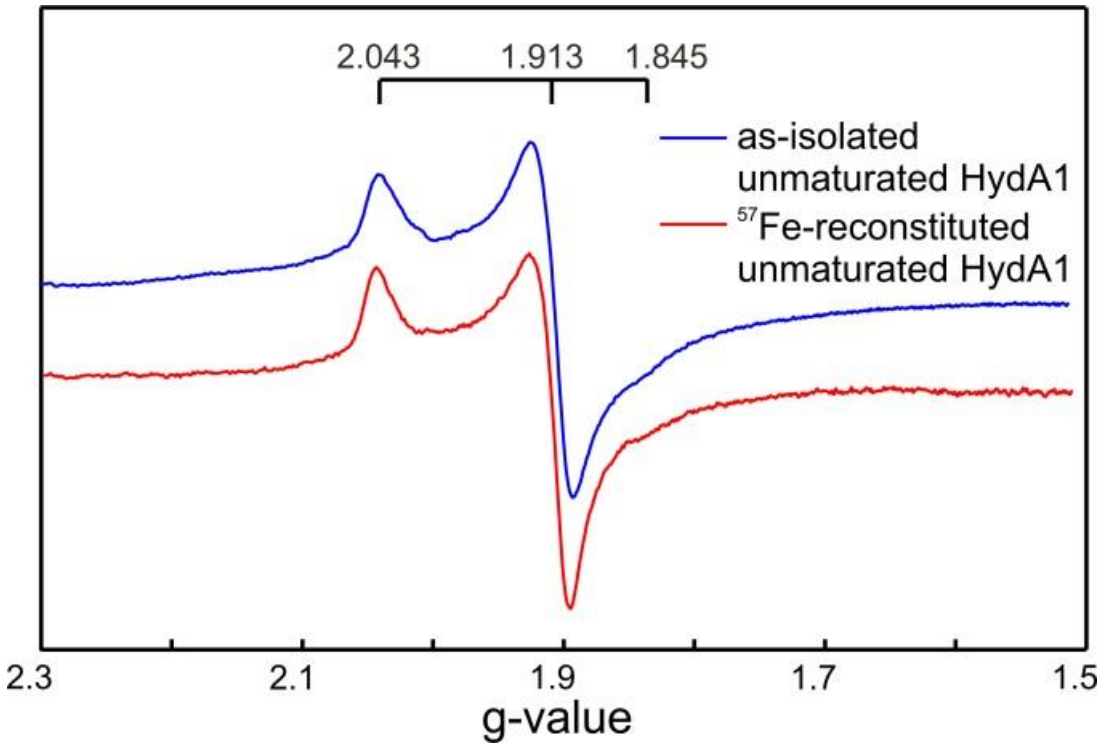

Figure S4. X-band CW EPR spectra of as-isolated unmaturated HydA1 (blue) and reconstituted unmaturated HydA1 (both reduced with 10 mM sodium dithionate). The experimental conditions are as following: 40 dB attenuation, ν_{mw} 9.65 GHz, time constant 40.96 ms, conversion time 81.92 ms, modulation amplitude 0.5 mT, modulation frequency 100 kHz, temperature 10 K.

EPR Spectroscopy

Table S1. Principal values of the ^{57}Fe hyperfine tensor of the H-cluster of [FeFe] hydrogenase in the H_{ox}-CO state

	A_1 (MHz)	A_2 (MHz)	A_3 (MHz)	$\lvert A_{iso} \rvert$ (MHz)	α (°)	β (°)	γ (°)	Ref.
Fe^1	2.2	5.5	5.5	4.4±0.3	0	0	0	this work
Fe^2	-1.7	2.8	2.8	1.3±0.3	0	30	90	
Fe^3	29.9	35.1	25.1	30.0±0.2	8	0	0	
Fe^4	31.2	37.3	31.2	33.2±0.2	0	0	0	
Fe^5	28.6	24.7	30.8	28.0±0.2	110	0	0	
Fe^6	23.5	29.6	29.8	27.6±0.2	20	0	0	
Fe_p	-2.2	-4.5	-5.3	4.0±0.1	110	25	44	*DdH*[5]
Fe_d	-1.7	+2.1	+2.1	0.8±0.1	0	30	90	
Fe^3	-30.4	-35.0	-35.4	33.6±0.15	90	185	0	
Fe^4	-30.7	-38.4	-34.5	34.5±0.2	90	5	0	
Fe^5	+30.3	+21.8	+27.8	26.7±0.2	6	110	0	
Fe^6	+30.2	+23.8	+26.7	27.0±0.2	76	-93	0	
Fe^1	-6.85	-6.85	-6.85	6.85±2				*D. vulgaris*[6]
Fe^2	0	0	0	0				
$Pair^1$	-30.95	-38.35	-32.19	33.8±2.7				
$Pair^2$	+27.94	+29.45	+31.50	29.6±1.35				
Fe^1+Fe^2				(–)9.5				CpI[7]
Pair1				+25.3				
Pair2				–28.3				

In this work the signs of the hyperfine couplings were not determined. Rows indicated in blue present values assigned to the $[2Fe]_H$ cluster and in green to the $[4Fe\text{-}4S]_H$ cluster. The most important parameter for comparison $\lvert A_{iso} \rvert$ is marked in orange.

Mössbauer spectroscopy

When compared to simulation 1 (Figure 4B), simulation 2 (Figure S5) has more similar quadrupole splitting ($\Delta E_Q 2(1)$ = 0.77 mm/s, $\Delta E_Q 2(2)$ = 0.60 mm/s) while the difference in isomer shifts ($\delta 2(1)$ = 0.21 mm/s, $\delta 2(2)$ = 0.04 mm/s) is larger:

Table S2. Mössbauer parameters

spectrum	component	δ (mm/s)	ΔE_Q (mm/s)	linewidth (mm/s)	relative intensity (%)
Figure 4A. $[4^{57}Fe\text{-}4S]_H$ H_{ox}-CO	$[4Fe\text{-}4S]_H$	0.42	1.04	0.57	64
	Fe(II) impurity	1.33	2.80	0.46	8
	FeS impurity	0.60	2.55	2.39	28
Figure 4B. $[2^{57}Fe]_H$ H_{ox}-CO simulation 1	$[2Fe]_H$ Fe1	0.16	0.89	0.41	46
	$[2Fe]_H$ Fe2	0.08	0.55	0.31	46
	Fe(II) impurity	1.32	2.83	0.81	8
Figure S5. $[2^{57}Fe]_H$ H_{ox}-CO simulation 2	$[2Fe]_H$ Fe1	0.21	0.77	0.40	45
	$[2Fe]_H$ Fe2	0.04	0.60	0.31	45
	Fe(II) impurity	1.15	3.18	0.71	10
Figure 4C. simulations $[2^{57}Fe]_H$ + $[4^{57}Fe\text{-}4S]_H$ H_{ox}-CO	$[2Fe]_H$ Fe1	0.16	0.89	0.41	16
	$[2Fe]_H$ Fe2	0.08	0.55	0.31	16
	$[4^{57}Fe\text{-}4S]_H$	0.42	1.04	0.57	68
Pereira et al.[6] $[4^{57}Fe\text{-}4S]_H$ + $[2^{57}Fe]_H$ H_{ox}-CO	$[4^{57}Fe\text{-}4S]_H$ 1	0.44	0.95		
	$[4^{57}Fe\text{-}4S]_H$ 2	0.41	0.98		
	$[2Fe]_H$ Fe1	0.17	0.70		
	$[2Fe]_H$ Fe2	0.13	0.65		

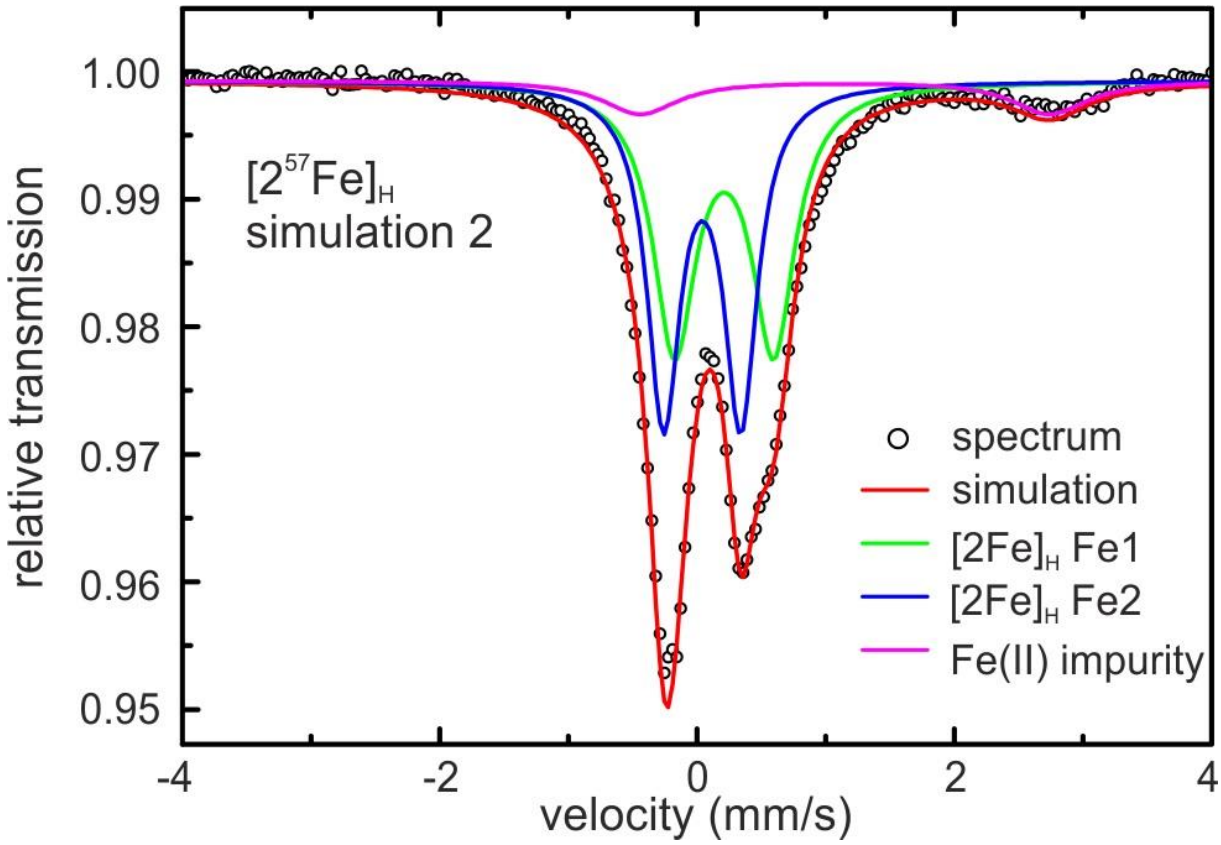

Figure S5. Mössbauer spectrum and simulation of H_{ox}-CO HydA1 selectively labeled with ^{57}Fe at the $[2Fe]_H$ subunit measured at 160 K. Shown here is the second possible simulation 2. Simulation 1 is shown in Figure 4B in the main text.

Nuclear Resonance Vibrational Spectroscopy (NRVS)

NRVS spectra are used to identify the vibrational modes associated with all ^{57}Fe sites. Fe-CN modes are generally found in the 400–500 cm^{-1} region of a NRVS spectrum. The NRVS spectrum for $(Et_4N)_2[^{57}Fe_2(adt)(CN)_2(CO)_4]$ displays two clear features in this region at 415 and 434 cm^{-1}, and the NRVS spectrum of $[2^{57}Fe]_H$ HydA1 H_{ox}-CO displays two features at 437 and 446 cm^{-1}. These features are assigned as Fe-CN modes and are the contributions from Fe-CN stretches and Fe-C-N bends. The clear blue shift of the Fe-CN modes upon incorporation of the precursor into the enzyme is indicative of either a strengthened Fe-CN bond, which increases the Fe-CN stretch energy, or a contribution from a higher energy Fe-C-N bend. As the $\nu_{C\equiv N}$ for $(Et_4N)_2[^{57}Fe_2(adt)(CN)_2(CO)_4]$ (2055 cm^{-1}) is lower in energy than the $\nu_{C\equiv N}$ for H_{ox}-CO (2090 and 2082 cm^{-1}, see Figure S2) the Fe-CN bond should be weaker when incorporated into the enzyme. This would be consistent with the one electron oxidation upon insertion resulting in less π back-bonding from the metal into the π* orbitals of the cyanide ligand. The higher Fe-CN mode energy must therefore be assigned to an increase in the energy of the Fe-C-N bends upon enzyme incorporation. The known hydrogen bonding of the cyanide ligands to the conserved lysine and serine residues in the enzyme active site (Lys358 and Ser232 in the [FeFe]-hydrogenase from *Clostridium pasteurianum*, CpI)[8] would explain this restriction and hence the energy increase in the Fe-CN modes.

Fe-CO modes are generally found in the 490–650 cm^{-1} region of an NRVS spectrum. The NRVS spectrum for $(Et_4N)_2[^{57}Fe_2(adt)(CN)_2(CO)_4]$ displays six peaks in the region of 490–650 cm^{-1} (at 516, 532, 576, 582, 603 and 653 cm^{-1} respectively). Fe-CO modes are at higher energy than the Fe-CN modes. This is as a result of strong π back-bonding from the iron to the π* orbital of the carbonyl ligand resulting in the Fe-CO having a more linear symmetry and hence higher energy.[9] The NRVS spectrum of $[2^{57}Fe]_H$ HydA1 H_{ox}-CO displays seven features in this region at 500, 530, 548, 557, 574, 587 and 603 cm^{-1}. It is notable that the Fe-CO modes are (on average) red shifted upon incorporation of the precursor into the enzyme. This is consistent with a one electron oxidation of the $[2Fe]_H$ subcluster, which results in less π back-bonding from the metal into the π* orbitals of the carbonyl ligand. It should also be noted that the redox change also causes a change in structure and symmetry of the molecule, thus causing the Fe-CO modes to red shift in the H_{ox}-CO spectra. This was also observed in *Pyrococcus furiosus* D14C ferredoxin.[10] Thus, the lines in the 500–600 cm^{-1} region correspond to symmetric and asymmetric stretching modes. The small features in the spectra at 557 and 587 cm^{-1} are representative of the in-plane and out-of-plane bending modes.

Fe-Fe (stretching and bending) bonds have previously been observed between 200–300 cm^{-1} for Fe-Fe model complexes, and $(Et_4N)_2[^{57}Fe_2(adt)(CN)_2(CO)_4]$ has a notable feature at 195 cm^{-1}. This feature is also observed in the $[^{57}Fe]_H$ HydA1 H_{ox}-CO enzyme at 197 cm^{-1}.[10] Features below 100 cm^{-1} are indicative of the Fe-S cluster torsional modes.[11]

References

1. Winter, G.; Thompson, D. W.; Loehe, J. R., Iron(II) Halides. In *Inorg. Syn.*, John Wiley & Sons, Inc.: New York, **2007**; pp 99-104.
2. Stanley, J. L.; Rauchfuss, T. B.; Wilson, S. R., *Organometallics* **2007,** *26*, 1907-1911.
3. Li, H.; Rauchfuss, T. B., *J. Am. Chem. Soc.* **2002,** *124*, 726-727.
4. Siebel, J. F.; Adamska-Venkatesh, A.; Weber, K.; Rumpel, S.; Reijerse, E.; Lubitz, W., *Biochemistry* **2015,** *54*, 1474-1483.
5. Silakov, A.; Reijerse, E. J.; Albracht, S. P. J.; Hatchikian, E. C.; Lubitz, W., *J. Am. Chem. Soc.* **2007,** *129*, 11447-11458.
6. Pereira, A. S.; Tavares, P.; Moura, I.; Moura, J. J. G.; Huynh, B. H., *J. Am. Chem. Soc.* **2001,** *123*, 2771 -2782.
7. Popescu, C. V.; Münck, E., *J. Am. Chem. Soc.* **1999,** *121*, 7877-7884.
8. Knörzer, P.; Silakov, A.; Foster, C. E.; Armstrong, F. A.; Lubitz, W.; Happe, T., *J. Biol. Chem.* **2012,** *287*, 1489-1499.
9. Kuchenreuther, J. M.; Guo, Y.; Wang, H.; Myers, W. K.; George, S. J.; Boyke, C. A.; Yoda, Y.; Alp, E. E.; Zhao, J.; Britt, R. D.; Swartz, J. R.; Cramer, S. P., *Biochemistry* **2012,** *52*, 818-826.
10. Mitra, D.; Pelmenschikov, V.; Guo, Y.; Case, D. A.; Wang, H.; Dong, W.; Tan, M.-L.; Ichiye, T.; Jenney, F. E.; Adams, M. W. W.; Yoda, Y.; Zhao, J.; Cramer, S. P., *Biochemistry* **2011,** *50*, 5220-5235.
11. Cramer, S.; Xiao, Y.; Wang, H.; Guo, Y.; Smith, M., *Hyperfine Interact* **2006,** *170*, 47-54.